https://doi.org/10.5194/egusphere-2024-1496
Preprint. Discussion started: 23 May 2024

Technical note: High-resolution analyses of concentrations and sizes of black carbon particles deposited on northwest Greenland over the past 350 years – Part 1. Continuous flow analysis of the SIGMA-D ice core using a Wide-Range Single-Particle Soot Photometer and a high-efficiency nebulizer

Kumiko Goto-Azuma[1,2], Remi Dallmayr[1,a], Yoshimi Ogawa-Tsukagawa[1], Nobuhiro Moteki[3], Tatsuhiro Mori[4], Sho Ohata[5], Yutaka Kondo[1], Makoto Koike[6], Motohiro Hirabayashi[1], Jun Ogata[1], Kyotaro Kitamura[1], Kenji Kawamura[1,2], Koji Fujita[5], Sumito Matoba[7], Naoko Nagatsuka[1,c], Akane Tsushima[1,b], Kaori Fukuda[1], and Teruo Aoki[1]

[1]National Institute of Polar Research, Tachikawa, Tokyo, 190-8518, Japan
[2]SOKENDAI, Shonan Village, Hayama, Kanagawa, 240-0193, Japan
[3]Tokyo Metropolitan University, Hachioji, Tokyo, 192-0397, Japan
[4]Keio University, Yokohama, Kanagawa, 223-8521, Japan
[5]Nagoya University, Nagoya, 464-8601, Japan
[6]University of Tokyo, Bunkyo-ku, 113-0033, Japan
[7]Hokkaido University, Sapporo, 060-0819, Japan
[a]Now at Alfred Wegener Institute for Polar and Marine Research, Bremerhaven, Germany
[b]Now at Meteorological Research Institute, Tsukuba, Ibaraki, 305-0052, Japan
[c]Now at Japan Agency for Marine-Earth Science and Technology, Yokosuka, Kanagawa, 237-0061, Japan

Correspondence to: Kumiko Goto-Azuma (kumiko@nipr.ac.jp)

Abstract. Ice cores can provide long-term records of black carbon (BC), an important aerosol species closely linked to the climate and environment. However, previous studies of ice cores only analysed BC particles with diameter of <600–850 nm, which could have led to underestimation of BC mass concentrations. Information on the size distribution of BC particles is very limited, and there are no Arctic ice core records of the temporal variation in BC size distribution. In this study, we applied a recently developed improved technique to analyse the BC concentration in an ice core drilled at the SIGMA-D site in northwest Greenland. The improved technique, which uses a modified Single-Particle Soot Photometer and a high-efficiency nebulizer, widens the measurable range of BC particle size. For high-resolution continuous analyses of ice cores, we developed a continuous flow analysis (CFA) system (resolution: 10–40 mm). Coupling of the improved BC measurement technique with the CFA system allows accurate high-resolution measurements of the size distribution and concentration of BC particles with diameter between 70 nm and 4 μm, with minimal particle losses. Using this technique, we reconstructed the size distributions

https://doi.org/10.5194/egusphere-2024-1496
Preprint. Discussion started: 23 May 2024

and the number and mass concentrations of BC particles during the past 350 years. On the basis of the size distributions, we assessed the underestimation of BC mass concentrations measured using the conventional method. For the period 2003–2013, the underestimation of the average mass concentration would have been 12%–17% for the SIGMA-D core.

1 Introduction

Black carbon (BC), which is emitted from both anthropogenic and natural sources (e.g., fossil fuel combustion and biomass burning), can affect Earth's radiation budget by absorbing sunlight and reducing the albedo of snow and ice surfaces (e.g., Bond et al., 2013; Mori et al., 2019; Matsui et al., 2022; Moteki, 2023 and references therein). Particles of BC can also affect cloud microphysical processes by acting as cloud condensation nuclei or ice nucleating particles (e.g., Bond et al., 2013; AMAP, 2021), thereby indirectly affecting the radiation budget. Over the past half-century, the Arctic has warmed at a rate four times faster than that of the global average (Rantanen et al., 2022), leading to drastic changes such as sea ice retreat, enhanced losses of glacier mass, and ecosystem changes. It is therefore important to evaluate the effects of BC on the radiation budget in the Arctic. Furthermore, BC emitted from fossil fuel combustion and large forest fires can affect air quality, ecosystems, and human health (Keane et al., 2008; Wang et al., 2021). Climate change can alter the frequency and magnitude of biomass burning events and hence influence BC emissions. In recent decades, global warming appears to have promoted increased occurrence of huge forest fires, which have triggered serious damage to forests, agriculture, and social infrastructure and sometimes even caused human casualties (Brown et al., 2023; Keeley and Syphard, 2021). Consequently accurate projections of the frequency and magnitude of future huge biomass burning events urgently need to be conducted to minimize the related potential hazard. To understand the effects of BC on the radiation budget and of the impacts of climate change on BC emissions, data acquired since the pre-industrial period are particularly valuable because we cannot fully understand the anthropogenic effects without characterizing BC in a pristine environment. Size distribution and concentration are important parameters that affect the radiative properties of BC particles. However, no direct measurements of the size distributions and concentrations of BC particles were performed prior to the past few decades despite numerous studies based on observations and aerosol/climate models (e.g., Bond et al., 2013 and references therein).

Ice cores can provide long-term records of BC deposition. Following development of the Single-Particle Soot Photometer (SP2; Droplet Measurement Technologies, USA) (Stephens et al., 2003; Baumgardner et al., 2004), it has been possible to measure BC in Arctic ice cores that contain very low concentrations of BC particles (McConnell et al., 2007;

https://doi.org/10.5194/egusphere-2024-1496
Preprint. Discussion started: 23 May 2024

Zdanowicz et al., 2018; Osmont et al., 2018; Zennaro et al., 2014) have become possible. Moreover, attachment of a coupled SP2 and nebulizer system to a continuous flow analysis (CFA) system allowed continuous and high temporal-resolution analyses of BC in ice cores drilled at a site with little summer melting (McConnell et al., 2007; Lim et al., 2017; Bisiaux et al., 2012a, 2012b). Many previous SP2 analyses of BC in ice cores, regardless of whether they used a CFA system, adopted the U5000AT ultrasonic nebulizer (Teledyne CETAC, USA) system (or a similar ultrasonic nebulizer) to aerosolize BC particles in melted ice core samples before their introduction to the SP2 (McConnell et al., 2007; Zennaro et al., 2014; Zdanowicz et al., 2018; Du et al., 2020; Kaspari et al., 2011; Wang et al., 2015; Bisiaux et al., 2012a, 2012b). Owing to the complex and temporally variable size dependence of the extraction efficiency of an ultrasonic nebulizer (Schwarz et al., 2012; Wendl et al., 2014; Ohata et al., 2013; Mori et al., 2016), large uncertainties are associated with the derived size distributions and concentrations. Obtaining accurate estimation of the size distribution of BC particles on a routine basis is not easy. Long-term ice core records of the size distribution of BC particles obtained using this type of nebulizer have not been reported. On the contrary, for BC particles with diameter of 100–1000 nm, a report indicates size-independent extraction efficiency (<15% variability) for the APEX Q jet nebulizer system (High-Sensitivity Sample Introduction System, Elemental Scientific Inc., USA) (Wendl et al., 2014). Using an APEX Q nebulizer system and an SP2 attached to a CFA system, Lim et al. (2017) analysed ice cores from Mt. Elbrus (western Caucasus Mountains) and reported temporal variability in the size and concentration of BC particles during 1825–2013. However, no BC size distribution data from Arctic ice cores have been published.

Snow and hence ice cores could contain much larger BC particles than those typically observed in the atmosphere (Schwarz et al., 2012, 2015). The particle size range typically measurable by an off-the-shelf SP2 (hereafter, the standard SP2) is from approximately 70 to 850–900 nm (Ohata et al., 2011; Mori et al., 2016), i.e., particles with diameter of >850–900 nm cannot be detected using the standard SP2. The extraction efficiency of the U5000AT ultrasonic nebulizer is 10%–12% for the particle diameter range of approximately 200–500 nm; it decreases sharply for diameters >500 nm and decreases to approximately 2% for particles with diameter of 700 nm (Ohata et al., 2013; Mori et al., 2016). Thus, measurements obtained using this nebulizer could have large uncertainties not only in size distribution but also in mass concentration if the ice core samples contain BC particles with diameter of >500 nm. Modern snow and ice core samples from the Arctic, including Greenland, do contain substantial fractions of BC particles with diameter of >600 nm (Mori et al., 2019). Mori et al. (2016) developed an improved technique for accurate measurement of the size distributions and concentrations of BC particles with

https://doi.org/10.5194/egusphere-2024-1496
Preprint. Discussion started: 23 May 2024

diameter between 70 nm and 4 μm in water samples. They used a Wide-Range SP2 (i.e., an SP2 modified to widen the measurable size range of BC particles) and a Marin-5 high-efficiency concentric pneumatic nebulizer (Teledyne CETAC, USA). For accurate, continuous, and high-resolution analyses of the concentrations and size distributions of BC particles in polar ice cores, we combined the improved BC measurement technique and a CFA system developed at the National Institute of Polar Research (NIPR). We used this system to analyse an ice core drilled at SIGMA-D in northwest Greenland (Matoba et al., 2015; Nagatsuka et al., 2021), following which we reconstructed the concentrations and size distributions of BC particles with diameter between 70 nm and 4 μm for the past 350 years. In this paper (called Part 1), we describe the coupled CFA-BC measurement system and the data that it produced. Using the new continuous high-resolution data, we investigated the seasonal variations in concentrations and size distributions of BC particles originating from both anthropogenic and biomass burning emissions and their temporal changes. In a companion paper (Part 2), we discuss the derived results.

2 Methods

2.1 Continuous flow analysis (CFA) system

To undertake high-resolution continuous analyses of ice cores, we developed a CFA system at NIPR. Figure 1 shows a schematic of the NIPR CFA system used to analyse the SIGMA-D core. It consists of a melting unit, debubbler unit, inductively coupled plasma–mass spectrometer (ICP-MS) unit, stable water isotope unit, microparticle unit, methane unit, and fraction collector unit in addition to a BC unit. The BC unit, ICP-MS unit, microparticle unit, and methane unit were added to an earlier version of the NIPR CFA system described by Dallmayr et al. (2016). The melting unit, debubbler unit, and the stable water isotope unit were the same as those used in the earlier version.

An ice core sample (cross section: 34 mm × 34 mm, length: ~0.5 m) was placed on a melt head inside a freezer. An 850 g weight was placed on top of the ice sample to allow stable melting. Before the ice core sample was completely melted, another similarly sized ice core sample was stacked on top of the first sample to maintain continuous melting of the ice samples. To promote melting, heaters are inserted into the melt head (Bigler et al., 2011; Osterberg et al., 2006). In the earlier NIPR CFA system, we used a melt head developed at the University of Maine (Osterberg et al., 2006). However, in this study, we used a melt head similar to the one used by Bigler et al. (2011) for the depth interval between 11.3 and 112.8 m of the SIGMA-D core. The University of Maine type melt head, designed principally for use in firn core analyses, is not airtight. For methane

https://doi.org/10.5194/egusphere-2024-1496
Preprint. Discussion started: 23 May 2024

analysis, we had to use an airtight melt head such as the one used by Bigler et al. (2011). For the depth interval between 6.1 and 11.3 m of the SIGMA-D core, we used the University of Maine type melt head (Dallmayr et al., 2016; Osterberg et al., 2006) to reduce water percolation through the porous firn caused by capillary action (Osterberg et al., 2006). For depths < 49.3 m, methane measurement was not performed.

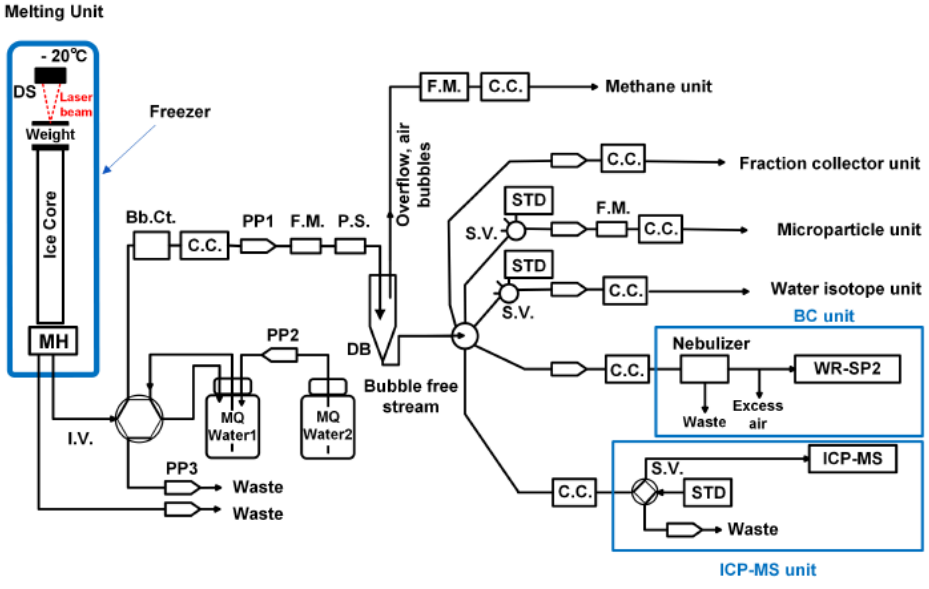

Figure 1: Schematic of the CFA system developed in this study.

DS: displacement sensor, MH: melt head, I.V.: injection valve, S.V.: selection valve, Bb.Ct.: bubble counter, C.C.: conductivity cell, PP: peristaltic pump, F.M.: flow meter, P.S. pressure sensor, DB: debubbler, STD: standard, MQ Water: ultra-pure water generated by a Milli-Q system.

The depth of an ice core sample is assigned using a laser positioning sensor (LKG-G505, Keyence, Japan), which determines the distance from the sensor to the top of the weight (Dallmayr et al., 2016). A typical melt speed, regulated by the voltage applied to the heaters in the melt head, is 30 mm min^{-1}. The depth resolution with this melt speed is approximately 0.3 ± 0.1 mm. The meltwater collected in the contamination-free inner part of the melt head is drawn through perfluoroalkoxy alkane tubing, an injection valve, and the debubbler unit by a peristaltic pump (Minipuls3 MP-2, Gilson, USA). Following removal of air bubbles by the debubbler unit, the meltwater is introduced to the different measurement units and to the fraction collector unit using peristaltic pumps (Reglo Digital ISM596, ISMATEC, Germany). Before each unit, an electrical

https://doi.org/10.5194/egusphere-2024-1496
Preprint. Discussion started: 23 May 2024

conductivity cell (conductivity meter Model 1056, Amber Science Inc., USA) is placed as close as possible to the unit to synchronise the depths of the ice core data acquired by the different measurement units and the depths of the meltwater samples collected by the fraction collector unit (McConnell et al., 2002; Dallmayr et al., 2016). A length of approximately 7 m of the ice core was melted once or twice a week.

The ICP-MS unit consists of an ICP-MS (7700 ICP-MS, Agilent Technologies, USA). The elements ^{23}Na, ^{24}Mg, ^{27}Al, ^{39}K, ^{43}Ca, and ^{56}Fe were each measured at a 3.00 s interval. Additionally, ^{89}Y was measured at a 3.00 s interval to check the stability of the ICP-MS. Data acquisition times for ^{23}Na, ^{24}Mg, ^{27}Al, ^{39}K, ^{43}Ca, ^{56}Fe, and ^{89}Y were 0.02, 0,1, 0.2, 0.1, 2.27, 0.252, and 0.044 s, respectively. In this study, we used mainly ^{23}Na data to date the core. The concentration of each of the elements was calibrated both before and after the CFA measurements of the day using a multi-element standard solution (XSTC-331, Spex CertiPrep, USA) diluted with ultra-pure water (Milli-Q water, Milli-Q Advantage, Merck Millipore, Germany). The detection limit, defined as [3σ of the blank value + the intercept of the calibration line], of ^{23}Na is 0.5 μg L^{-1}.

The stable water isotope unit is same as that used by Dallmayr et al. (2016). It consists of a vaporization module (Gkinis et al., 2011; Dallmayr et al., 2016) and a wavelength-scanned cavity ring-down spectrometer (L2130-i, Picarro Inc., USA). We calibrated the spectrometer by analysing three sets of laboratory water isotope standards after the CFA measurements of the day (Dallmayr et al., 2016). These laboratory standards were calibrated with VSMOW2 and SLAP2 standards purchased from the International Atomic Energy Agency. Details of calibrations and the performance of the stable water isotope unit have been described in a previous study (Dallmayr et al., 2016).

The NIPR CFA system includes a microparticle unit, methane unit, and fraction collector unit consisting of three fraction collectors. However, we do not discuss them further here because the data that they provided are not relevant. The specification and performance of each of these units will be reported elsewhere.

2.2 Black carbon unit

We applied the improved technique developed by Mori et al. (2016) to the BC unit of the NIPR CFA system. The BC unit consists of a Wide-Range SP2 (Mori et al., 2016) and a concentric pneumatic nebulizer (Marin-5, Teledyne CETAC, USA). The SP2 detects the incandescence signal from individual BC particles induced by irradiation of an Nd-YAG laser (Stephens et al., 2003; Baumgardner, 2004; Schwarz et al., 2006). The standard SP2 can detect BC particles with diameter of between

https://doi.org/10.5194/egusphere-2024-1496
Preprint. Discussion started: 23 May 2024

70 and 850–900 nm, assuming BC particle density of 1.8 g cm^{-3} (Moteki and Kondo, 2010). For the Wide-Range SP2, Mori et al. (2016) expanded the upper limit of the measurable diameter to 4 μm by modifying the detection unit of the standard SP2. Hence, the Wide-Range SP2 can detect BC particles with diameter of between 70 nm and 4 μm. The meltwater that passes through the debubbler unit is fed to the Marin-5 nebulizer at a constant flow rate of 6.3 μL s^{-1} by a peristaltic pump (REGLO Digital ISM596, ISMATEC, Germany). We used G3 Grade air as a carrier gas for the nebulizer. The flow rate of the carrier gas is 15.2 cm^3 s^{-1} at standard temperature and pressure (i.e., 0 °C and 1013 hPa, respectively). The nebulizer converts a fraction of the meltwater into water droplets that are immediately heated to 140 °C in a spray chamber, generating a mixture of BC particles, non-BC particles, and water vapor. After the non-aerosolized meltwater is removed via the drains, this mixture is cooled to 3 °C in a condenser, thereby removing the water vapor. Hence, only BC and non-BC particles are introduced to the Wide-Range SP2 at a flow rate of 12 cm^3 min^{-1}. The details of the Wide-Range SP2 and the Marin-5, together with assessment of their performance, have been reported by Mori et al. (2016).

To derive the relationship between the peak incandescence signal and the mass of each BC particle (Stephens et al., 2003; Schwarz et al., 2006), we used fullerene soot (Alpha Aesar Inc., USA, Lot No. 20W054) as a standard material (Moteki and Kondo, 2010). We used an Aerosol Particle Mass Analyzer (Moteki and Kondo, 2010) Model 3601 (APM-II, KANOMAX, Japan) to extract fullerene soot particles with a mass range of 1.19–203 fg, corresponding to mass equivalent diameters of 100–600 nm. Following Mori et al. (2016), we produced two calibration curves for BC masses below and above 10 fg, which corresponds to the mass equivalent diameter of 220 nm. Mass equivalent diameters of BC particles were calculated assuming a BC particle density of 1.8 g cm^{-3} (Moteki and Kondo, 2010).

For accurate measurement of BC particle size, the nebulizer efficiency and its size dependence must be known (Ohata et al., 2013; Mori et al., 2016). However, to the best of our knowledge, previous ice core studies using an SP2 rarely considered nebulizer efficiency, except those conducted by Wendl et al. (2014) and Lim et al. (2017). We determined nebulizer efficiency using Polystyrene Latex Sphere (PSL) suspensions with known number concentrations (Ohata et al., 2011, 2013; Mori et al., 2016) for diameters of >200 nm. We used PSL particles supplied by two manufacturers. The diameters of the PSL particles supplied by Polysciences Inc., USA (NIST Traceable Particle Size Standard), were 207, 288, 505, 603, 707, 814, 1025, and 1537 nm, and the diameters of those supplied by Thermo Fisher Scientific Inc., USA, were 2000 and 3000 nm. For diameters of <200 nm, we used AquaBlack 162 (AB-162, Tokai Carbon Co. Ltd., Japan), which is a laboratory standard for BC particles suspended in water (Mori et al., 2016; Ohata et al., 2011; Ohata et al., 2013). The number concentration of the PSL particles

https://doi.org/10.5194/egusphere-2024-1496
Preprint. Discussion started: 23 May 2024

and that of the AquaBlack samples in the carrier gas were measured by the Wide-Range SP2, and compared with those of the PSL suspensions and the B-162 suspensions, respectively, to calculate nebulizer efficiency. Measurements of the PLS suspensions were performed with the SP2 laser currents lower than those for BC measurements.

Number and mass concentrations of BC particles in the melted ice core samples were calculated using the nebulizer efficiency (Mori et al., 2016). The combination of the Wide-Range SP2 and the Marin-5 nebulizer provides a measurable diameter range of 70 nm to 4 μm. With this BC unit attached to the melting and debubbler units, we acquired number concentrations, mass concentrations, and mass equivalent diameters of BC particles every second. Using the same definition of the detection limit mentioned above (Sect. 2.1), we determined the detection limits of BC number and mass concentrations in water samples to be approximately 10 counts·L^{-1} and 0.01 μg·L^{-1}, respectively. The accuracy of the BC number and mass concentrations in the water samples was approximately 16%, which was derived from the measurement uncertainties of the peristaltic pump flow rate (±5%), nebulizer flow rate (±5%), nebulizer efficiency (±10%), and BC concentration in the carrier gas measured by the SP2 (±10%) (Mori et al., 2016, 2021). The reproducibility of the number and mass concentrations for repeated measurements of the same melted ice core and Arctic snow samples was usually better than 10% (Mori et al., 2019). Additionally, possible changes in the count median diameter during the nebulizing process were estimated to be only 2 nm for the fullerene soot, whose count median diameter was ~120 nm and whose mass concentration in water was 6.9–64 μg·L^{-1} (Mori et al., 2016). A similar value was estimated for the AB-162. These experimental results suggest that the shape of the BC size distribution and the BC mass concentration changed little during the nebulizer extraction process.

BC particles could stick to the various components of the system such as the melt head, debubbler, valves, conductivity cells, tubing, and nebulizer, which could reduce the concentration and change the size distribution. We investigated whether losses of BC particles occurred in the CFA system. We injected a melted surface snow sample from SIGMA-A (northwest Greenland) (Matoba et al., 2018) at the melt head, and measured the concentration and size distribution of BC particles. We used the University of Copenhagen type melt head for this test. We also injected the same sample directly into the Marin-5 nebulizer and measured the concentration and size distribution of BC particles. We then compared the results of the two experiments to check whether any changes occurred that could be attributed to the CFA system.

2.3 Signal dispersion tests

https://doi.org/10.5194/egusphere-2024-1496
Preprint. Discussion started: 23 May 2024

The mixing of meltwater, which occurs in parts of the system such as the melt head, debubbler, valves, conductivity cells, tubing, and nebulizer, causes signal dispersion and reduces the resolution of the CFA data. To evaluate the signal dispersion, we examined the response of each unit by switching between injection of ultra-pure water and injection of standard solutions or melted ice core/snow samples at the melt heads (Bigler et al., 2011). The ultra-pure water used in this study was made using a Milli-Q Advantage system (Merck Millipore, Germany). The samples used for the dispersion tests are listed in Table 1.

Table 1. List of samples for signal dispersion tests

Measurement	Type of test samples
BC	AquaBlack 162 (AB-162, Tokai Carbon Co. Ltd.)
ICP-MS	Surface snow from Dome Fuji, Antarctica, concentrated by heating
Water stable isotopes	A shallow ice core drilled at Dome Fuji, Antarctica (JARE52 core)

2.4 Processing and analyses of the SIGMA-D ice core

A 222.7 m ice core was drilled at the SIGMA-D site (77.636° N, 59.120° W; 2100 m a.s.l.) in northwest Greenland in spring 2014 (Matoba et al., 2015). The annual mean air temperature and accumulation rate at the site were estimated to be −25.6 °C and 0.23 w eq yr^{-1} (Nagatsuka et al., 2021), respectively. In the field, the top 175.77 m of the core was divided into two vertical sections (Sections A and B).

Section A was kept frozen and transported to NIPR in Japan. We analysed the depth interval between 6.1 and 112.87 m of this section using the CFA system described in Sect. 2.1 and 2.2. The top 6.1 m of this section was too fragile to be analysed with the CFA system; hence, we manually cut segments of approximately 0.1 m. These discrete samples were decontaminated in a cold room (−20 °C) using a precleaned ceramic knife, and then placed in powder-free plastic bags. They were then melted and transferred to precleaned glass and polypropylene bottles in a class 10,000 clean room. The samples in glass bottles were analysed for stable water isotopes and BC. The BC was analysed using a Wide-Range SP2 (Mori et al., 2016) and a concentric pneumatic nebulizer (Marin-5, Teledyne CETAC, USA), i.e., the same as those in the NIPR CFA system. The setting and analytical conditions of the Wide-Range SP2 and Marin-5 were similar to those described in Sect. 2.2. Concentrations and diameters of BC particles were calibrated in the same way as described in Sect. 2.2.

Stable isotopes of water for the discrete samples were analysed using a near-infrared cavity ring-down spectrometer

https://doi.org/10.5194/egusphere-2024-1496
Preprint. Discussion started: 23 May 2024

(L2120-i, Picarro, Inc. USA), a high-precision vaporizer (A0211, Picarro Inc., USA), and an autosampler (PAL HTC9 - xt - LEAP, LEAP Technologies, USA). The precision of determination was ±0:05‰ for $\delta^{18}O$. The samples in polypropylene bottles were analysed for six elements (^{23}Na, ^{24}Mg, ^{27}Al, ^{39}K, ^{40}Ca, and ^{56}Fe) with an ICP-MS (7700 ICP-MS, Agilent Technologies, USA) in a class 10,000 clean room at NIPR.

Section B was cut in the field into 0.06–0.12 m long vertical segments for the top 5 m of the core, 0.05–0.08 m long segments for depths of 5–12 m, and approximately 0.05 m long segments for the depth interval between 12 and 112.87 m. Each segment was placed in a plastic bag, melted, and transferred to a precleaned polypropylene bottle in the field. The discrete samples contained in the polypropylene bottles were refrozen in the field, transported to Japan, and kept frozen until analysis, whereupon they were melted and analysed for major ions and stable water isotopes (Nagatsuka et al., 2021). Samples from depths above 61.2 m were analysed for Na^+, K^+, Mg^{2+} and Ca^{2+}, Cl^-, NO_3^-, and SO_4^{2-} with two ion chromatographs (ICS-2100, Thermo Fisher Scientific, USA) at Hokkaido University, Japan, whereas samples from depths between 61.2 and 112.87 m were analysed for NH_4^+, Na^+, K^+, Mg^{2+}, Ca^{2+}, Cl^-, NO_3^-, and SO_4^{2-} with two ion chromatographs (ICS-2000, Thermo Fisher Scientific, USA) at NIPR. The limit of detection of Na^+ measured at Hokkaido University was 1 $\mu g \cdot L^{-1}$, and that measured at NIPR was 0.2 $\mu g \cdot L^{-1}$. Stable water isotopes were analysed for all samples from Section B using a near-infrared cavity ring-down spectrometer (L2130-i, Picarro Inc., USA) and a high-throughput vaporizer (A0212, Picarro Inc., USA) at Hokkaido University. The precision of determination was ±0:08‰ for $\delta^{18}O$. For dating purposes, tritium concentrations were measured using a liquid scintillation counter (LSC-LB3; Aloka Co. Ltd., Japan) at 0.05 m intervals for the depth interval of 19.15–26.47 m (Nagatsuka et al., 2021).

3 Results and Discussion

3.1 Nebulizer efficiency

Figure 2 shows the efficiency of the Marin-5 nebulizer for different flow rates of meltwater. As previously reported (Mori et al., 2016), nebulizer efficiency depends on flow rate. For three flow rates—0.192, 0.384, and 0.478 $mL \cdot min^{-1}$—the efficiency was almost constant for diameters of <2000 nm, and it declined linearly with diameter for diameters >2000 nm, as reported by Mori et al. (2016). For a flow rate of 0.384 $mL \cdot min^{-1}$, which is the flow rate used in the NIPR CFA system, the efficiency was 34.2% ± 8.0% for particles with diameter of <2000 nm, and it declined linearly with diameter for diameters of 2–4 µm.

https://doi.org/10.5194/egusphere-2024-1496
Preprint. Discussion started: 23 May 2024

249

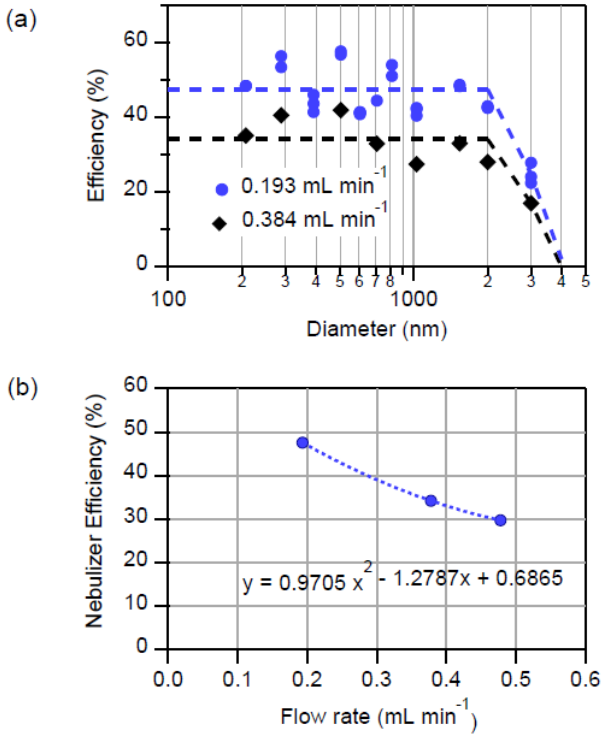

Figure 2: Dependence of nebulizer efficiency on (a) BC diameter for two flow rates and (b) flow rate for BC diameter of <2 µm.

250 **3.2 Signal dispersion**

251 Figure 3 displays the results of dispersion tests for $\delta^{18}O$, Na, and BC. We defined two types of response times: (1) the time
252 (t1) required for transition from 10% of the standard (or ice core/snow sample) value to 90% of the standard (or ice core/snow
253 sample) value, and (2) the time (t2) required for transition from 90% of the standard (or ice core/snow sample) value to 10%
254 of the standard (or ice core/snow sample) value. The baseline was determined as the value for Milli-Q water. Response times
255 t1 and t2 depend on how the data are smoothed owing to noise in the data signal. Table 2 shows examples of t1 and t2 when
256 the data are smoothed by taking 5-point running means. Neither t1 nor t2 depends on the standard (or ice core/snow sample)
257 concentrations or values (Bigler et al., 2011). For BC, we present normalized values together with concentrations in Fig. 3 to
258 illustrate how we determined t1 and t2. We converted t1 and t2 to depth intervals L1 and L2, respectively, assuming a constant
259 melt speed of 30 mm s^{-1}. In Table 2, we list the averages of L1 and L2 for a rise of 10%–90% and decay of 90%–10%,

https://doi.org/10.5194/egusphere-2024-1496
Preprint. Discussion started: 23 May 2024

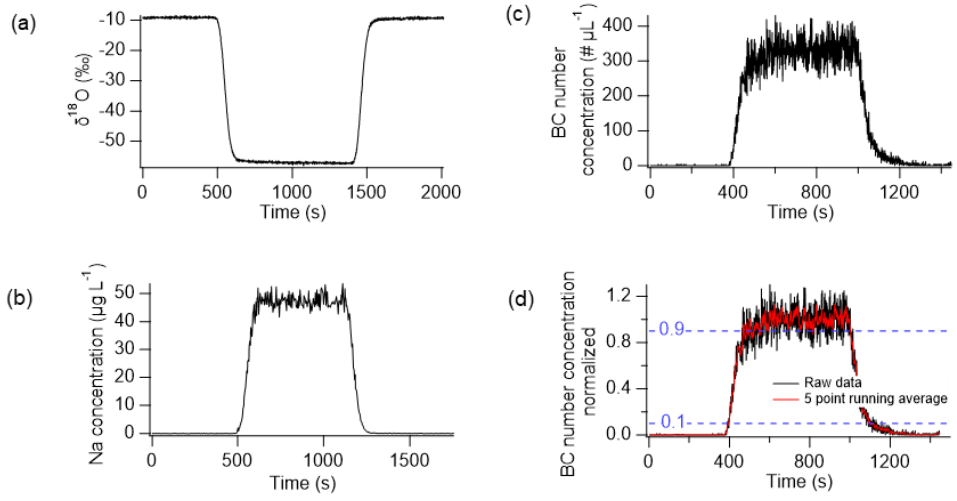

Figure 3: Results of dispersion tests: (a) $\delta^{18}O$, (b) Na concentration, (c) BC number concentration, and (d) normalized BC number concentration. Black and red lines represent raw data and 5 point running averages, respectively. Blue dotted lines show 0.1 and 0.9 levels.

respectively. L1 and/or L2 are often defined as the depth resolution of a CFA system (Bigler et al., 2011; Erhardt et al., 2023; Grieman et al., 2022). However, the resolution of our CFA system is better than these values. We could resolve two peaks located at distances closer than the resolution defined in this way. For $\delta^{18}O$, Na, and BC, peaks 10 mm apart are usually resolved. For BC and Na, L2 is slightly greater than L1, indicating that the melting direction affects the CFA signal (Breton et al., 2012). The CFA signal for BC and Na might not be symmetrical, even if a concentration peak is symmetrical along the core depth (Breton et al., 2012). Conversely, $\delta^{18}O$ shows similar L1 and L2 values, indicating that melting direction does not affect the CFA signal.

Table 2 Results of dispersion tests

	University of Copenhagen type melt head					University of Maine type melt head				
	t1 (s)	t2 (s)	L1 (mm)	L2 (mm)	Average of L1 & L2 (mm)	t1 (s)	t2 (s)	L1 (mm)	L2 (mm)	Average of L1 & L2 (mm)
$\delta^{18}O$	78	75	39	37.5	38.3	75	81	37.5	40.5	39
BC number concentration	67	90	33.5	45	39.3	105	124	52.5	62	57.3
Na concentration	66	74	33	37	35	57	89	28.5	44.5	36.5

https://doi.org/10.5194/egusphere-2024-1496
Preprint. Discussion started: 23 May 2024

3.3 Minimal losses of BC particles in the NIPR CFA system

Figure 4 and Table 3 present the results of BC loss tests. The sample injected at the melt head, which then flowed through the CFA system, produced mass and number size distributions of BC particles consistent with those derived following direct injection. The mass and number concentrations of BC particles injected at the melt head were 94% and 102% of those determined following direct injection. Thus, the BC concentrations of the two types of injections agreed within the bounds of uncertainty of the BC measurements. Therefore, we can conclude that minimal loss of BC particles occurs in the NIPR CFA system.

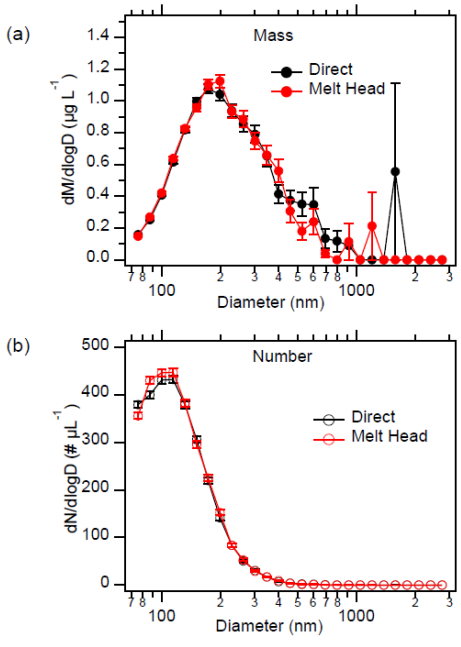

Figure 4: Comparison of direct injection of a surface snow sample collected at SIGMA-A to Marin-5 and injection at the melt head. (a) Mass and (b) number size distributions of BC shown for direct and melt head injections. Error bars indicate $\pm 1\sigma$ of a Poisson distribution.

Table 3 Results of BC loss test using a surface snow sample from SIGMA-A, northwest Greenland

	Melt head blank	Injection at melt head	Direct injection	Ratio of injection at melt head/direct injection
BC mass concentration (μg L^{-1})	0.004	0.623	0.660	0.944
BC number concentration (# L^{-1})	0.1	175.8	173.0	1.016

https://doi.org/10.5194/egusphere-2024-1496
Preprint. Discussion started: 23 May 2024

276

277 **3.4 Chronology of the SIGMA-D ice core**

278 Figure 5a compares the raw $\delta^{18}O$ data obtained from the CFA system and those obtained from the discrete sample analysis.
279 Figure 5b compares the raw Na concentration data obtained from the CFA system using ICP-MS, and the Na^+ concentration
280 data from discrete sample analysis using ion chromatography. The CFA and discrete measurements agree well for $\delta^{18}O$ and
281 Na. The values of Mg, K, and Ca from the CFA analysis (not shown) also agree well with the values of Mg^{2+}, K^+, and Ca^{2+}
282 from the discrete sample analysis, respectively (not shown).

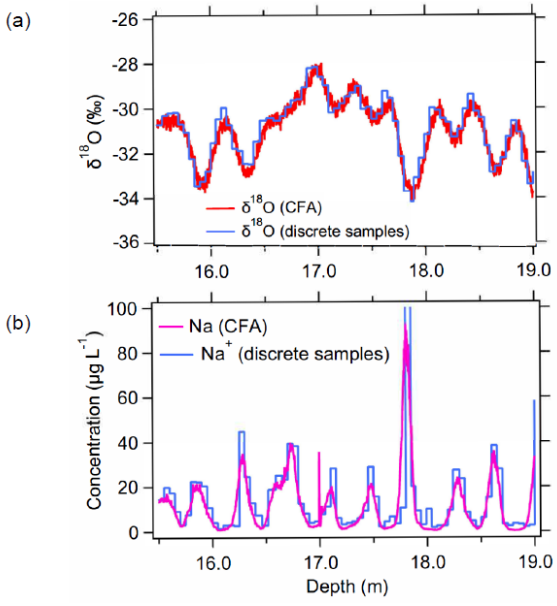

Figure 5: Comparison of CFA measurements and discrete sample measurements of the SIGMA-D core.

284 The CFA data from Section A and the discrete data from Section B agree well, and therefore we adopted the
285 chronology of Section B reported by Nagatsuka et al. (2021) to analyse the BC data from Section A. Because Na^+ (and Na)
286 and $\delta^{18}O$ show regular seasonal peaks in winter and summer, respectively, the dating was based on annual layer counting using
287 mainly Na^+ and $\delta^{18}O$ data from the discrete samples cut from Section B. We also used a tritium peak and volcanic SO_4^{2-} peaks
288 as reference horizons. However, for the years before 1783, we made minor adjustments where high SO_4^{2-} peaks did not match
289 the volcanic eruptions reported following analysis of other Greenland ice cores (Sigl et al., 2018). For the depth intervals where
290 seasonal variability of Na^+ and $\delta^{18}O$ data were ambiguous, we supplementarily used seasonal variability of Ca, which is
291 originated from mineral dust and shows seasonal peaks in late-winter to early spring (e.g., Nakazawa et al., 2021; Kuramoto

https://doi.org/10.5194/egusphere-2024-1496
Preprint. Discussion started: 23 May 2024

et al., 2011; Dibb et al., 2007), obtained from the CFA system. The uncertainties of dating were estimated to be less than ±2 years. The CFA data covered the years 1653–2002.

3.5 High-resolution BC data from the SIGMA-D ice core

Figure 6 displays the raw data of BC mass and number concentrations acquired using the CFA system at 1 s interval corresponding to a depth interval of 0.0005 m, together with the 10 mm averages of the data. The raw mass concentration data frequently exceed 50 $\mu g \cdot L^{-1}$. However, as can be deduced from the differences in mass concentrations and number concentrations, the sporadic high concentration peaks in the raw mass concentration data could have been formed by only a small number of large BC particles, which would result in the noise evident in the data. To reduce the noise, we calculated the 10 mm averages of the data, corresponding to a 1–2 week interval depending on the depth of the core. The 10 mm averages of the mass concentrations often exceed 10 $\mu g \cdot L^{-1}$.

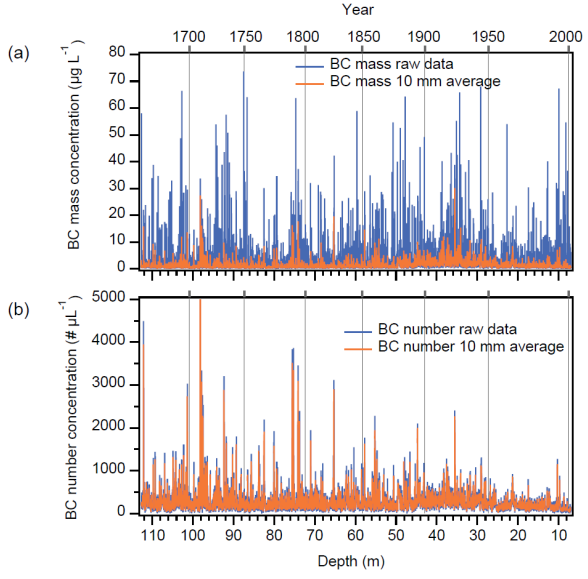

Figure 6: (a) Mass and (b) number concentrations of BC in the SIGM-D core. Raw data and 10 mm averages of the raw data are shown in blue and red, respectively.

The upper limit of the measurable BC diameters would affect the BC mass concentrations if the ice core samples contain a large proportion of large particles. As described in Sect. 2.2, the upper limit of the NIPR BC unit is 4 μm, whereas that of a measurement system using the standard SP2 is 850 nm at best. If a measurement system uses a nebulizer such as the

https://doi.org/10.5194/egusphere-2024-1496
Preprint. Discussion started: 23 May 2024

U5000AT ultrasonic nebulizer (Teledyne CETAC, USA), which was used in many previous studies, nebulizer efficiency is drastically reduced for diameters greater than approximately 500 nm (Mori et al., 2016), which would lead to underestimation of BC mass concentrations if the ice core contains a large proportion of BC particles with diameter of >500 nm. We calculated the number and mass size distributions of BC particles averaged over different periods. As an example, the 11-year mean normalized number and mass size distributions for 2003–2013, derived from analyses of the discrete samples, are plotted in Fig. 7. It is evident from Fig. 7 that the total number concentrations of BC particles would not have been affected by the upper limits of the measurable BC diameters, which were between approximately 600 and 850 nm in previous studies. In contrast, the mass concentrations would have been underestimated by 17% and 12% for upper limits of 650 and 850 nm, respectively.

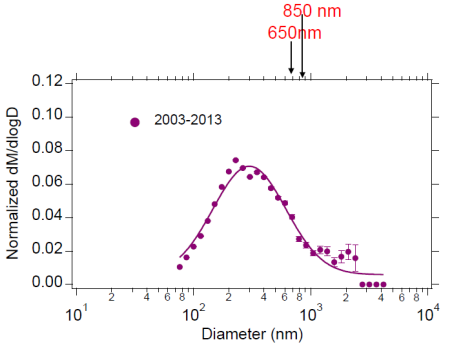

Ratio of BC mass concentration 650nm/Total	Ratio of BC number concentration 650nm/Total	Ratio of BC mass concentration 850nm / Total	Ratio of BC number concentration 850nm / Total
0.83	1.00	0.88	1.00

Figure 7: Averaged mass and number size distribution for the period 2003–2013. Error bars indicate ±1σ of a Poisson distribution. The table shows ratios of concentrations for upper limits of 650 and 850 nm to total.

To examine the impact of large BC particles in the SIGMA-D ice core, the BC mass concentrations averaged for 10 mm intervals, assuming different upper limits, are plotted in Fig. 8a. In Fig. 8b, the ratios of the BC mass concentrations for different upper limits versus the total BC mass concentrations are shown. Figure 8b shows that the standard SP2 combined with a high-efficiency nebulizer such as the Marin-5 of the APEX-Q, which would give an upper limit of 850 nm, would occasionally underestimate the BC mass concentration by 10% or more. However, using a nebulizer such as the U5000AT nebulizer, whose efficiency depends substantially on the diameter of BC particles, the upper limit would be approximately 600–650 nm, and we would frequently underestimate the BC mass concentration by 80% or more. Figure 9 presents histograms of the ratios of BC mass concentrations for upper limits of 650 and 850 nm. For the upper limit of 650 nm, 36% of the 10 mm

https://doi.org/10.5194/egusphere-2024-1496
Preprint. Discussion started: 23 May 2024

323 averages account for <90% of the total BC mass concentrations; for the upper limit of 850 nm, 15% of the 10 mm averages

324 account for <90% of the total BC mass concentrations.

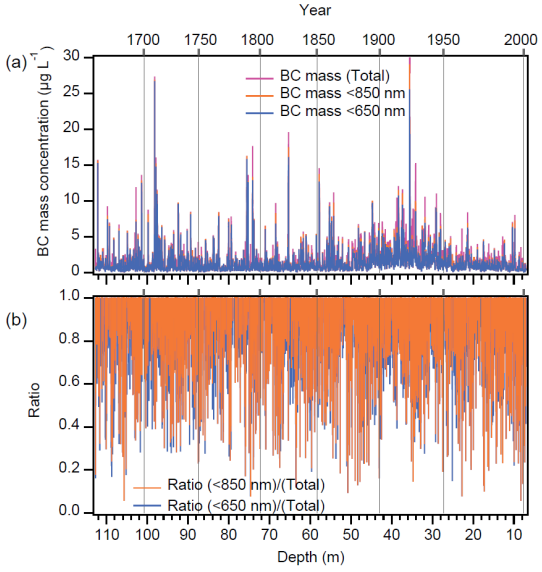

Figure 8: Comparison of BC mass concentration (10 mm averages) in the SIGMA-D core for different upper limits of BC diameters. (a) Total concentration measured in this study (upper limit: 4 um), concentration for upper limit of 850 nm, and concentration for upper limit of 650 nm are displayed in pink, red, and blue colors, respectively. (b) Ratio of BC mass concentration for upper limits of 850 nm (red) and 650 nm (blue) to total concentration.

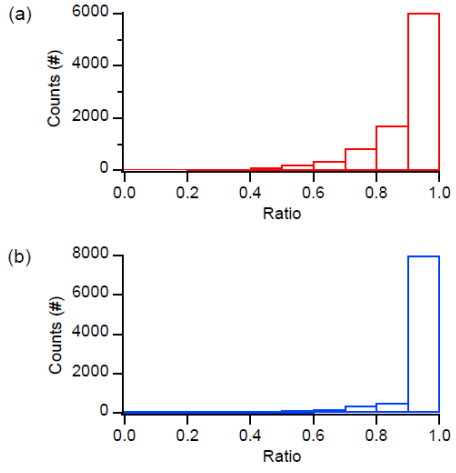

Figure 9: Histograms of underestimation for 10 mm averaged data. Horizontal axis represent the ratio of mass concentration for an upper limit of (a) 650 nm and (b) 850 nm. Vertical axis represents the number of 10 mm averaged data in each ratio bin.

https://doi.org/10.5194/egusphere-2024-1496
Preprint. Discussion started: 23 May 2024

4. Conclusions

We developed a CFA system and incorporated a BC unit that uses the improved BC measurement technique developed by Mori et al. (2016). The CFA system can acquire continuous and high-resolution measurements of the number and mass concentrations of BC, and the size distribution of BC particles, in addition to stable water isotopes ($\delta^{18}O$ and δD), six elements (^{23}Na, ^{24}Mg, ^{27}Al, ^{39}K, ^{43}Ca, and ^{56}Fe), microparticles, electrical conductivity, and methane. There were minimal losses of BC particles within the NIPR CFA system. We analysed the SIGMA-D ice core retrieved from northwest Greenland using this newly developed system. If we define the depth resolution as the average of the rise of 10%–90% and decay of 90%–10% of the CFA signal, the resolutions were 38, 39, and 35 mm for $\delta^{18}O$, BC, and Na, respectively. These depth resolutions correspond to the temporal resolutions of 0.08–0.16, 0.11–0.23, and 0.07–0.15 years for $\delta^{18}O$, BC, and Na, respectively, depending on depth. However, we could usually resolve two peaks that were approximately 10 mm apart, corresponding to 0.5–1.0 week depending on depth. We were able to analyse monthly resolved BC data as described in the companion paper, i.e., Part 2 of our study on BC in the SIGMA-D core.

The Wide-Range SP2 and the Marin-5 nebulizer allowed analysis of BC particles with diameter between 70 nm and 4 μm, contrasting with the analysis of BC particles with diameter of between 70 and 600–850 nm reported in previous studies. This enabled us to reconstruct accurate mass concentrations and size distributions of BC particles, together with their temporal changes (Goto-Azuma et al., submitted), which could contribute to estimation of the impacts of BC on the radiation budget and cloud microphysics. Using the size distribution data, we estimated the extent of underestimation that would be caused by (1) a combination of the standard SP2 and a high efficiency nebulizer, and (2) a combination of the standard SP2 and a traditional ultrasonic nebulizer. For (1), approximately 15% of the 10 mm averaged data from the SIGMA-D core accounted for <90% of the total BC mass concentrations. For (2), approximately 36% of the 10 mm averaged data from the SIGMA-D core accounted for <90% of the total BC mass concentrations. The extent of the underestimation depends on depth and thus on the age of the core. For the period 2003–2013, (1) and (2) would lead to underestimation of the averaged mass concentration by 12% and 17%, respectively. Although few ice core studies have considered the size distribution of BC and estimated the extent of underestimation of BC mass concentrations, the present-day snow from Svalbard (Mori et al., 2019) and an ice core from Mt. Elbrus in the western Caucasus Mountains (Lim et al., 2017) do contain non-negligible amounts of BC particles with

https://doi.org/10.5194/egusphere-2024-1496
Preprint. Discussion started: 23 May 2024

diameter of >650 nm. Therefore, the improved method for accurate measurement of BC mass concentrations should be used to properly constrain aerosol models.

Data availability

The data used in this study will be submitted to the Arctic Data Archive System when the manuscript has been published.

Author contributions

KGA designed the study and led the manuscript writing. RD, MH, KGA, and KeK built the CFA system at NIPR. NM, TM, SO, YK, and MK developed the improved method for BC analyses, including the calibration method. YOT, RD, JO, and KyK performed the CFA analyses of the SIGMA-D core. SM, KoF, NN, and AT dated the core. KGA, YOT, and KaF analysed the CFA data. MH and SM measured ion concentrations. TA designed and led the ice coring project at SIGMA-D. All the authors discussed the results.

Competing interests

The authors declare that they have no conflict of interest.

Acknowledgements

We would like to thank Hideaki Motoyama who drilled the SIGMA-D core, and Yuki Komuro who cut and processed the core in the field. We would also like to thank Kazuhiro Hayashi who assisted the dispersion tests. We are grateful to the University of Copenhagen and the University of Maine for providing us with the melt head designs. This study has been supported by the JSPS KAKENHI (Grant Numbers: JP 22221002, JP23221004, and JP18H04140), the Arctic Challenge for Sustainability (ArCS) Project (Program Grant Number: JPMXD130000000)), the Arctic Challenge for Sustainability II (ArCS II) Project (Program Grant Number: JPMXD1420318865), and the Environment Research and Technology Development Funds (JPMEERF20172003, JPMEERF20202003 and JPMEERF20232001) of the Environmental Restoration and Conservation Agency of Japan. We thank James Buxton MSc, from Edanz (https://jp.edanz.com/ac), for editing a draft of this manuscript.

https://doi.org/10.5194/egusphere-2024-1496
Preprint. Discussion started: 23 May 2024

References

AMAP: Arctic Climate Change Update 2021: Key Trends and Impacts, Summary for Policy-makers, 2021.

Baumgardner, D.: Warming of the Arctic lower stratosphere by light absorbing particles, Geophys. Res. Lett., 31, 10.1029/2003gl018883, 2004.

Baumgardner, D., Kok, G., and Raga, G.: Warming of the Arctic lower stratosphere by light absorbing particles, Geophys. Res. Lett., 31, https://doi.org/10.1029/2003GL018883, 2004.

Bigler, M., Svensson, A., Kettner, E., Vallelonga, P., Nielsen, M. E., and Steffensen, J. P.: Optimization of high-resolution continuous flow analysis for transient climate signals in ice cores, Environ. Sci. Technol., 45, 4483–4489, 10.1021/es200118j, 2011.

Bisiaux, M. M., Edwards, R., McConnell, J. R., Albert, M. R., Anschütz, H., Neumann, T. A., Isaksson, E., and Penner, J. E.: Variability of black carbon deposition to the East Antarctic Plateau, 1800–2000 AD, Atmos. Chem. Phys., 12, 3799–3808, 10.5194/acp-12-3799-2012, 2012a.

Bisiaux, M. M., Edwards, R., McConnell, J. R., Curran, M. A. J., Van Ommen, T. D., Smith, A. M., Neumann, T. A., Pasteris, D. R., Penner, J. E., and Taylor, K.: Changes in black carbon deposition to Antarctica from two high-resolution ice core records, 1850–2000 AD, Atmos. Chem. Phys., 12, 4107–4115, 10.5194/acp-12-4107-2012, 2012b.

Bond, T. C., Doherty, S. J., Fahey, D. W., Forster, P. M., Berntsen, T., DeAngelo, B. J., Flanner, M. G., Ghan, S., Kärcher, B., Koch, D., Kinne, S., Kondo, Y., Quinn, P. K., Sarofim, M. C., Schultz, M. G., Schulz, M., Venkataraman, C., Zhang, H., Zhang, S., Bellouin, N., Guttikunda, S. K., Hopke, P. K., Jacobson, M. Z., Kaiser, J. W., Klimont, Z., Lohmann, U., Schwarz, J. P., Shindell, D., Storelvmo, T., Warren, S. G., and Zender, C. S.: Bounding the role of black carbon in the climate system: A scientific assessment, J. Geophys. Res.-Atmos., n/a-n/a, 10.1002/jgrd.50171, 2013.

Breton, D. J., Koffman, B. G., Kurbatov, A. V., Kreutz, K. J., and Hamilton, G. S.: Quantifying signal dispersion in a hybrid ice core melting system, Environ. Sci. Technol., 46, 11922–11928, 10.1021/es302041k, 2012.

Brown, P. T., Hanley, H., Mahesh, A., Reed, C., Strenfel, S. J., Davis, S. J., Kochanski, A. K., and Clements, C. B.: Climate warming increases extreme daily wildfire growth risk in California, Nature, 621, 760-766, 10.1038/s41586-023-06444-3, 2023.

Dallmayr, R., Goto-Azuma, K., Kjær, H. A., Azuma, N., Takata, M., Schüpbach, S., and Hirabayashi, M.: A high-resolution continuous flow analysis system for polar ice cores, B. Glaciol. Res., 34, 11–20, 10.5331/bgr.16R03, 2016.

https://doi.org/10.5194/egusphere-2024-1496
Preprint. Discussion started: 23 May 2024

Dibb, J. E., Whitlow, S. I., and Arsenault, M.: Seasonal variations in the soluble ion content of snow at Summit. Greenland: Constraints from three years of daily surface snow samples, Atmos. Environ., 41, 5007–5019, 10.1016/j.atmosenv.2006.12.010, 2007.

Du, Z.-H., Xiao, C.-D., Dou, T.-F., Li, C.-J., Ding, M.-H., Sharma, S., Ma, X.-Y., Wang, S.-M., and Zhang, W.-B.: A shallow ice core from East Greenland showing a reduction in black carbon during 1990–2016, Adv. Clim. Change Res., 11, 360–369, https://doi.org/10.1016/j.accre.2020.11.009, 2020.

Erhardt, T., Jensen, C. M., Adolphi, F., Kjær, H. A., Dallmayr, R., Twarloh, B., Behrens, M., Hirabayashi, M., Fukuda, K., Ogata, J., Burgay, F., Scoto, F., Crotti, I., Spagnesi, A., Maffezzoli, N., Segato, D., Paleari, C., Mekhaldi, F., Muscheler, R., Darfeuil, S., and Fischer, H.: High-resolution aerosol data from the top 3.8-kyr of the East Greenland Ice coring Project (EGRIP) ice core, Earth Syst. Sci. Data, 15, 5079–5091, 10.5194/essd-15-5079-2023, 2023.

Gkinis, V., Popp, T. J., Blunier, T., Bigler, M., Schupbach, S., Kettner, E., and Johnsen, S. J.: Water isotopic ratios from a continuously melted ice core sample, Atmos. Meas. Tech., 4, 2531–2542, 10.5194/amt-4-2531-2011, 2011.

Grieman, M. M., Hoffmann, H. M., Humby, J. D., Mulvaney, R., Nehrbass-Ahles, C., Rix, J., Thomas, E. R., Tuckwell, R., and Wolff, E. W.: Continuous flow analysis methods for sodium, magnesium, and calcium detection in the Skytrain ice core, J. Glaciol., 68, 90–100, 10.1017/jog.2021.75, 2022.

Kaspari, S. D., Schwikowski, M., Gysel, M., Flanner, M. G., Kang, S., Hou, S., and Mayewski, P. A.: Recent increase in black carbon concentrations from a Mt. Everest ice core spanning 1860–2000 AD, Geophys. Res. Lett., 38, L04703, 10.1029/2010gl046096, 2011.

Keane, R. E., Agee, J. K., Fulé, P., Keeley, J. E., Key, C., Kitchen, S. G., Miller, R., and Schulte, L. A.: Ecological effects of large fires on US landscapes: benefit or catastrophe?, Int. J. Wildland Fire, 17, 696–712, https://doi.org/10.1071/WF07148, 2008.

Keeley, J. E. and Syphard, A. D.: Large California wildfires: 2020 fires in historical context, Fire Ecol., 17, 22, 10.1186/s42408-021-00110-7, 2021.

Kuramoto, T., Goto-Azuma, K., Hirabayashi, M., Miyake, T., Motoyama, H., Dahl-Jensen, D., and Steffensen, J. P.: Seasonal variations of snow chemistry at NEEM, Greenland, Ann. Glaciol., 52, 193–200, 10.3189/172756411797252365, 2011.

https://doi.org/10.5194/egusphere-2024-1496
Preprint. Discussion started: 23 May 2024

Lim, S., Faïn, X., Ginot, P., Mikhalenko, V., Kutuzov, S., Paris, J. D., Kozachek, A., and Laj, P.: Black carbon variability since preindustrial times in the eastern part of Europe reconstructed from Mt. Elbrus, Caucasus, ice cores, Atmos. Chem. Phys., 17, 3489–3505, 10.5194/acp-17-3489-2017, 2017.

Matoba, S., Motoyama, H., Fujita, K., Yamasaki, T., Minowa, M., Onuma, Y., Komuro, Y., Aoki, T., Yamaguchi, S., Sugiyama, S., and Enomoto, H.: Glaciological and meteorological observations at the SIGMA-D site, northwestern Greenland Ice Sheet, B. Glaciol. Res., 33, 7‑14, 10.5331/bgr.33.7, 2015.

Matoba, S., Niwano, M., Tanikawa, T., Iizuka, Y., Yamasaki, T., Kurosaki, Y., Aoki, T., Hashimoto, A., Hosaka, M., and Sugiyama, S.: Field activities at the SIGMA-A site, northwestern Greenland Ice Sheet, 2017, B. Glaciol. Res., 36, 15–22, 10.5331/bgr.18R01, 2018.

Matsui, H., Mori, T., Ohata, S., Moteki, N., Oshima, N., Goto-Azuma, K., Koike, M., and Kondo, Y.: Contrasting source contributions of Arctic black carbon to atmospheric concentrations, deposition flux, and atmospheric and snow radiative effects, Atmos. Chem. Phys., 22, 8989–9009, 10.5194/acp-22-8989-2022, 2022.

McConnell, J. R., Lamorey, G. W., Lambert, S. W., and Taylor, K. C.: Continuous ice-core chemical analyses using inductively coupled plasma mass spectrometry, Environ. Sci. Technol., 36, 7–11, 10.1021/es011088z, 2002.

McConnell, J. R., Edwards, R., Kok, G. L., Flanner, M. G., Zender, C. S., Saltzman, E. S., Banta, J. R., Pasteris, D. R., Carter, M. M., and Kahl, J. D.: 20th-century industrial black carbon emissions altered Arctic climate forcing, Science, 317, 1381–1384, 10.1126/science.1144856, 2007.

Mori, T., Moteki, N., Ohata, S., Koike, M., Goto-Azuma, K., Miyazaki, Y., and Kondo, Y.: Improved technique for measuring the size distribution of black carbon particles in liquid water, Aerosol Sci. Tech., 50, 242–254, 10.1080/02786826.2016.1147644, 2016.

Mori, T., Goto-Azuma, K., Kondo, Y., Ogawa-Tsukagawa, Y., Miura, K., Hirabayashi, M., Oshima, N., Koike, M., Kupiainen, K., Moteki, N., Ohata, S., Sinha, P. R., Sugiura, K., Aoki, T., Schneebeli, M., Steffen, K., Sato, A., Tsushima, A., Makarov, V., Omiya, S., Sugimoto, A., Takano, S., and Nagatsuka, N.: Black carbon and inorganic aerosols in Arctic snowpack, J. Geophys. Res.-Atmos., 124, 13325–13356, 10.1029/2019jd030623, 2019.

Mori, T., Kondo, Y., Ohata, S., Goto-Azuma, K., Fukuda, K., Ogawa-Tsukagawa, Y., Moteki, N., Yoshida, A., Koike, M., Sinha, P. R., Oshima, N., Matsui, H., Tobo, Y., Yabuki, M., and Aas, W.: Seasonal variation of wet deposition of black

https://doi.org/10.5194/egusphere-2024-1496
Preprint. Discussion started: 23 May 2024

carbon at Ny-Ålesund, Svalbard, J. Geophys. Res.-Atmos., 126, e2020JD034110, https://doi.org/10.1029/2020JD034110, 2021.

Moteki, N.: Climate-relevant properties of black carbon aerosols revealed by in situ measurements: a review, Prog. Earth Planet. Sci., 10, 12, 10.1186/s40645-023-00544-4, 2023.

Moteki, N. and Kondo, Y.: Dependence of laser-induced incandescence on physical properties of black carbon aerosols: Measurements and theoretical interpretation, Aerosol Sci. Tech., 44, 663–675, 10.1080/02786826.2010.484450, 2010.

Nagatsuka, N., Goto-Azuma, K., Tsushima, A., Fujita, K., Matoba, S., Onuma, Y., Dallmayr, R., Kadota, M., Hirabayashi, M., Ogata, J., Ogawa-Tsukagawa, Y., Kitamura, K., Minowa, M., Komuro, Y., Motoyama, H., and Aoki, T.: Variations in mineralogy of dust in an ice core obtained from northwestern Greenland over the past 100 years, Clim. Past, 17, 1341–1362, 10.5194/cp-17-1341-2021, 2021.

Nakazawa, F., Nagatsuka, N., Hirabayashi, M., Goto-Azuma, K., Steffensen, J. P., and Dahl-Jensen, D.: Variation in recent annual snow deposition and seasonality of snow chemistry at the east Greenland ice core project (EGRIP) camp, Greenland, Polar Sci., 27, 100597, https://doi.org/10.1016/j.polar.2020.100597, 2021.

Ohata, S., Moteki, N., and Kondo, Y.: Evaluation of a method for measurement of the concentration and size distribution of black carbon particles suspended in rainwater, Aerosol Sci. Tech., 45, 1326–1336, 10.1080/02786826.2011.593590, 2011.

Ohata, S., Moteki, N., Schwarz, J., Fahey, D., and Kondo, Y.: Evaluation of a method to measure black carbon particles suspended in rainwater and snow samples, Aerosol Sci. Technol., 47, 1073–1082, 10.1080/02786826.2013.824067, 2013.

Osmont, D., Wendl, I. A., Schmidely, L., Sigl, M., Vega, C. P., Isaksson, E., and Schwikowski, M.: An 800-year high-resolution black carbon ice core record from Lomonosovfonna, Svalbard, Atmos. Chem. Phys., 18, 12777–12795, 10.5194/acp-18-12777-2018, 2018.

Osterberg, E. C., Handley, M. J., Sneed, S. B., Mayewski, P. A., and Kreutz, K. J.: Continuous ice core melter system with discrete sampling for major ion, trace element, and stable isotope analyses, Environ. Sci. Technol., 40, 3355–3361, 10.1021/es052536w, 2006.

Rantanen, M., Karpechko, A. Y., Lipponen, A., Nordling, K., Hyvärinen, O., Ruosteenoja, K., Vihma, T., and Laaksonen, A.: The Arctic has warmed nearly four times faster than the globe since 1979, Commun. Earth Environ., 3, 168, 10.1038/s43247-022-00498-3, 2022.

https://doi.org/10.5194/egusphere-2024-1496
Preprint. Discussion started: 23 May 2024

Schwarz, J. P., Gao, R. S., Fahey, D. W., Thomson, D. S., Watts, L. A., Wilson, J. C., Reeves, J. M., Darbeheshti, M., Baumgardner, D. G., Kok, G. L., Chung, S. H., Schulz, M., Hendricks, J., Lauer, A., Kärcher, B., Slowik, J. G., Rosenlof, K. H., Thompson, T. L., Langford, A. O., Loewenstein, M., and Aikin, K. C.: Single-particle measurements of mid-latitude black carbon and light-scattering aerosols from the boundary layer to the lower stratosphere, J. Geophys. Res., 111, D16207, 10.1029/2006jd007076, 2006.

Schwarz, J. P., Doherty, S. J., Li, F., Ruggiero, S. T., Tanner, C. E., Perring, A. E., Gao, R. S., and Fahey, D. W.: Assessing Single Particle Soot Photometer and Integrating Sphere/Integrating Sandwich Spectrophotometer measurement techniques for quantifying black carbon concentration in snow, Atmos. Meas. Tech., 5, 2581–2592, 10.5194/amt-5-2581-2012, 2012.

Schwarz, J. P., Perring, A. E., Markovic, M. Z., Gao, R. S., Ohata, S., Langridge, J., Law, D., McLaughlin, R., and Fahey, D. W.: Technique and theoretical approach for quantifying the hygroscopicity of black-carbon-containing aerosol using a single particle soot photometer, J. Aerosol Sci., 81, 110–126, http://dx.doi.org/10.1016/j.jaerosci.2014.11.009, 2015.

Sigl, M., Abram, N. J., Gabrieli, J., Jenk, T. M., Osmont, D., and Schwikowski, M.: 19th century glacier retreat in the Alps preceded the emergence of industrial black carbon deposition on high-alpine glaciers, The Cryosphere, 12, 3311–3331, 10.5194/tc-12-3311-2018, 2018.

Stephens, M., Turner, N., and Sandberg, J.: Particle identification by laser-induced incandescence in a solid-state laser cavity, Appl. Opt., 42, 3726–3736, 10.1364/AO.42.003726, 2003.

Wang, M., Xu, B., Kaspari, S. D., Gleixner, G., Schwab, V. F., Zhao, H., Wang, H., and Yao, P.: Century-long record of black carbon in an ice core from the Eastern Pamirs: Estimated contributions from biomass burning, Atmos. Environ., 115, 79–88, https://doi.org/10.1016/j.atmosenv.2015.05.034, 2015.

Wang, D., Guan, D., Zhu, S., Kinnon, M. M., Geng, G., Zhang, Q., Zheng, H., Lei, T., Shao, S., Gong, P., and Davis, S. J.: Economic footprint of California wildfires in 2018, Nat. Sustain., 4, 252–260, 10.1038/s41893-020-00646-7, 2021.

Wendl, I. A., Menking, J. A., Färber, R., Gysel, M., Kaspari, S. D., Laborde, M. J. G., and Schwikowski, M.: Optimized method for black carbon analysis in ice and snow using the Single Particle Soot Photometer, Atmos. Meas. Tech., 7, 2667–2681, 10.5194/amt-7-2667-2014, 2014.

Zdanowicz, C. M., Proemse, B. C., Edwards, R., Feiteng, W., Hogan, C. M., Kinnard, C., and Fisher, D.: Historical black carbon deposition in the Canadian High Arctic: a >250-year long ice-core record from Devon Island, Atmos. Chem. Phys., 18, 12345–12361, 10.5194/acp-18-12345-2018, 2018.

https://doi.org/10.5194/egusphere-2024-1496
Preprint. Discussion started: 23 May 2024

508 Zennaro, P., Kehrwald, N., McConnell, J. R., Schüpbach, S., Maselli, O. J., Marlon, J., Vallelonga, P., Leuenberger, D.,
509 Zangrando, R., Spolaor, A., Borrotti, M., Barbaro, E., Gambaro, A., and Barbante, C.: Fire in ice: two millennia of boreal
510 forest fire history from the Greenland NEEM ice core, Clim. Past, 10, 1905–1924, 10.5194/cp-10-1905-2014, 2014.

511

512